respect to y and applying the continuity conditions valid at the structure's interfaces to the implied components, the (transformed) components $\bar{H}_{yi}(k_y)$ and $\bar{H}_{zi}(k_y)$ can be expressed in terms of $\bar{E}_{oy}(k_y)$ and $\bar{E}_{oz}(k_y)$.

Formulating eqn. 1 in the spectral, k_y, domain by means of Parseval's theorem and inserting the components $\bar{H}_{yi}$ and $\bar{H}_{zi}$ into it, the final stationary formula can be obtained.

Omitting the 'sandwich' layer ($\varepsilon_r' = 1$), the following simple formula for the propagation constant or equivalently for the effective dielectric constant $\varepsilon_{reff} = (\beta/K_0)^2$ of the double-sided slotline[1] is derived:

$$\int_0^\infty \left[(1 - \varepsilon_{yeff})\gamma_2^{-1} + (\varepsilon_r - \varepsilon_{reff}) \times \tanh\left(\gamma_1 \frac{h}{2}\right)\gamma_1^{-1} \right] |\bar{E}_{0y}|^2 \, dk_y = 0 \quad (2)$$

with $\gamma_1^2 = \beta^2 + k_y^2 - \varepsilon_r \kappa_0^2$ and $\gamma_2^2 = \beta^2 + k_y^2 - k_0^2$. k_0 is the wavenumber in vacuum. For deriving eqn. 2 the longitudinal slot field component E_{oz} is assumed to be negligible when compared with E_{oy}.

Numerical results: In order to obtain numerical results from eqn. 2, the Fourier transform of E_{oy} must be available. Extrapolating from the corresponding static configuration, the following formula for E_{oy} is considered an approximation.

$$E_{oy} = \frac{1}{\sqrt{\left[1 - \left(\frac{y}{s/2}\right)^2\right]}} \quad (3)$$

Its Fourier transform can be given in closed form

$$\bar{E}_{oy} = -\frac{s}{2} - \pi J_0\left(-\frac{s}{2} - k_y\right) \quad (4)$$

J_0 is the Bessel function of the first kind, zero order. Eqn. 2 can now be evaluated in a straightforward way using well-known methods for the numerical integration and the root determination. For facilitating the comparison with results published elsewhere, the dispersion characteristic in Fig. 2 shows the normalised slotline wavelength $(\lambda_g/\lambda_o) = \varepsilon_{reff}^{-1/2}$ against the normalised slot-width (s/λ_0). There is very good agreement between the results in Fig. 2 ($h/\lambda_0 = 0{\cdot}0305$) and the results in Reference 1. It may be mentioned here that the low-permittivity, wide-slot configurations are of main interest for the antenna arrays applications.

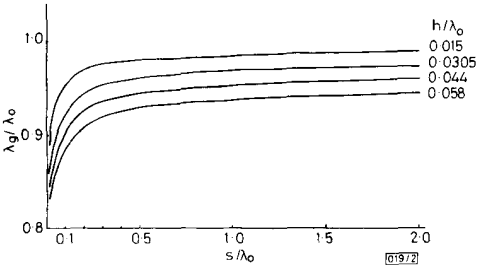

Fig. 2 *Wavelength against slot width*
$\varepsilon_r = 2{\cdot}22$

Conclusion: A quite simple and efficient procedure for computing the dispersion characteristic (propagation constant) of the double-sided single microslot on the base of a stationary formula, along with numerical results of practical interest, has been presented.

S. G. PINTZOS
Research Centre of Hellenic Navy (Geten)
Ministry of Defence
Holargos, Athens, Greece

23rd March 1990

References

1 COETZEE, J. C., and MALHERBE, J. A. G.: 'Dispersion characteristics for double-sided slotlines', *Electron. Lett.*, 1989, **25**, pp. 1383–1385
2 PREGLA, R., and PINTZOS, S. G.: 'Determination of the propagation constants in coupled microslots by a variational method'. Proc. 5th Colloquium Microwave Communication, Budapest, 1974, pp. 491–500 (MT)
3 DONN, C.: 'A miniature, circularly polarized cross-slotline antenna'. IEEE AP-S Int. Symp. Digest, 1989, pp. 1328–1331
4 JANASWAMY, R., and SCHAUBERT, D. H.: 'Dispersion characteristics for wide slotlines on low permittivity substrates', *IEEE Trans.*, 1985, **MTT-33**, pp. 723–726
5 JANASWAMY, R., and SCHAUBERT, D. H.: 'Characteristic impedance of a wide slotline on low permittivity substrates', *IEEE Trans.*, 1986, **MTT-34**, pp. 900–902

SINGLE ENDED RESONANT POWER SUPPLY FOR INDUCTION HEATING

Indexing terms: Circuit theory and design, Power supply circuits

Details are given of a zero current switched Class E prototype power supply suitable for small scale induction heating applications. The unit operates with a maximum frequency of 40 kHz providing a peak output power of 3 kW using a single GTO device.

Introduction: Small scale induction heating applications require solid state power sources which can provide up to 3 kW of high frequency power from a single phase 50 Hz supply. The frequency range is determined by the requirement to operate above the audible level and also by the frequency limitations of the switching devices. Operation between 20 and 40 kHz is common especially with domestic induction heating units.

The output coil is obviously inductive in nature and resonant output circuits are required.

If direct-off-line working is envisaged, then the presence of a resonant circuit means that the switching device will be subjected to high voltages and current. This would indicate that a device such as a high speed GTO was therefore appropriate, especially if circuit commutated gate assisted techniques are used.

Power circuit design: Many resonant circuit topologies have been proposed and attempts have been made to apply these to induction heating.[1,2] The circuit shown in Fig. 1 is a zero current circuit similar to the Class E topology. Since this

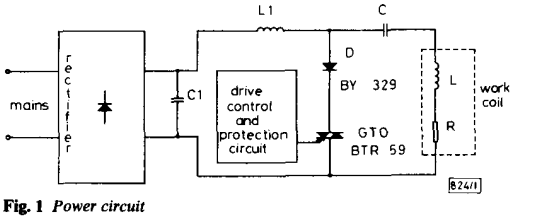

Fig. 1 *Power circuit*

circuit can operate in a zero current mode over its input voltage range the input can be taken from the rectified mains without smoothing. This avoids the problems of harmonic generation and poor input power factor.

The work coil parameters L and R are determined by the dimensions and electromagnetic properties of the workpiece. In this case $L = 41{\cdot}47\,\mu$H and $R = 7{\cdot}86\,\Omega$. A circuit design strategy has been developed to calculate the component values for optimum circuit operation. In this case the values calculated were $L_i = 208\,\mu$H and $C = 130{\cdot}5$ nF.

The inverter was supplied directly from the single phase mains via a full bridge diode rectifier but without smoothing. A relatively small filter capacitor, C_f (1 μF), was included to protect the mains from high frequency interference.

The control and protection circuitry is shown in Fig. 2. Fig. 3 shows the basic waveforms required to explain their operation. The operating frequency was set by a voltage controlled oscillator (VCO). Monostable MS1 produced a short positive pulse at the GTO anode current zero crossing point, detected by a zero current detector ZCD.

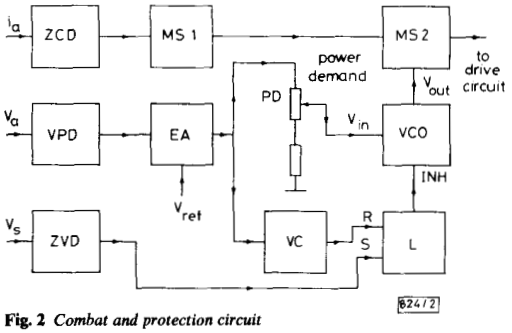

Fig. 2 *Combat and protection circuit*

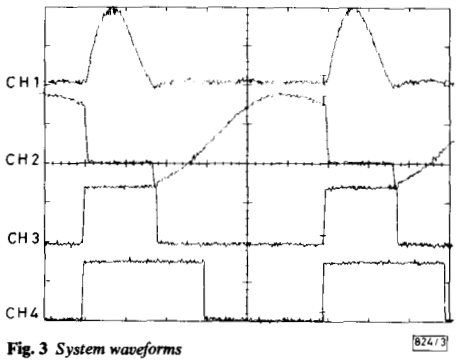

Fig. 3 *System waveforms*
CH1: i_a (20 A/div)
CH2: V_a (500 V/div)
CH3: V_{ms2} (10 V/div)
CH4: V_{eca} (10 V/div)
Time: 5 μs/div

The control circuit output pulse was produced by monostable MS2. It was initiated by the positive edge of the VCO output pulse, t_0, and terminated with the positive edge of MS1 output pulse, t_1. In this way zero current switching of the GTO was obtained within the operating frequency range and the device switching losses minimised.

The peak voltage across the GTO, V_{ap}, was constantly monitored by the voltage peak detector (VPD). If V_{ap} does not exceed the maximum limit set by the reference voltage, V_{REF}, the error amplifier EA is fully saturated.

The output power could be varied from 3 kW peak power down to 600 W peak power using the potentiometer P which varied the VCO output frequency between approximately 30 and 40 kHz.

If the work coil was unloaded V_{ap} rose sharply, EA came out of saturation and its output voltage and hence the circuit operating frequency had to be reduced to keep V_{ap} within safe limits. When the EA voltage reached a value of 1·5 V, the voltage comparator VC set the latch L to 1 and the VCO was shut down. The latch L was reset when the supply voltage V_s fell to zero.

In practice an operating frequency of 26 kHz corresponded to an unloaded inverter and an output power of 60 W which was dissipated in the work coil. At this point the inverter would be shut down.

Tests on prototype: The prototype was nominally rated at 3 kW peak output power and maximum operating frequency of 40 kHz. Figs. 4 and 5 show the GTO voltage and current waveforms at maximum and minimum power, respectively. The peak voltage across the GTO at maximum power was 950 V and the peak current was 65 A.

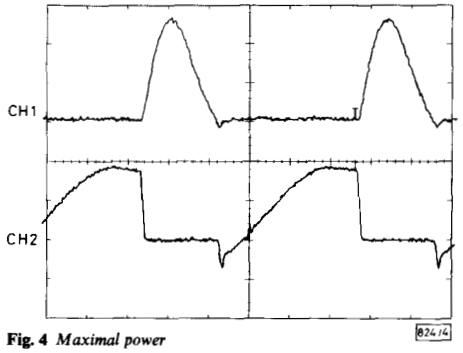

Fig. 4 *Maximal power*
CH1: i_a (20 A/div)
CH2: V_a (500 V/div)
Time: 5 μs/div

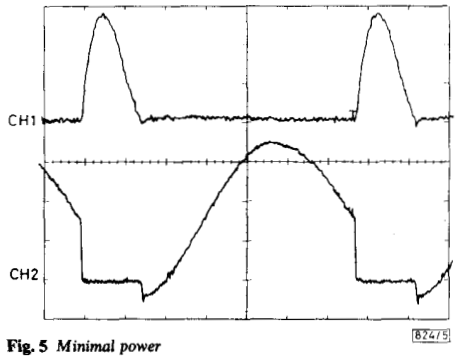

Fig. 5 *Minimal power*
CH1: i_a (10 A/div)
CH2: V_a (200 V/div)
Time: 5 μs/div

If the workpiece was fully removed at maximum power output the protection circuitry was able to shut down the power supply before the voltage across the GTO exceeded 1 kV.

The relationship between the power output of the induction heating power supply and the switching frequency of the GTO is shown in Fig. 6. The range of frequency required for power control was relatively small (26–40 kHz) and input filter requirements were therefore substantially reduced.

Conclusions: A prototype power supply was built, and full power control and protection circuitry was implemented. The design was simple, and therefore cheap, and reduced harmonic generation problems which are of ever increasing importance.

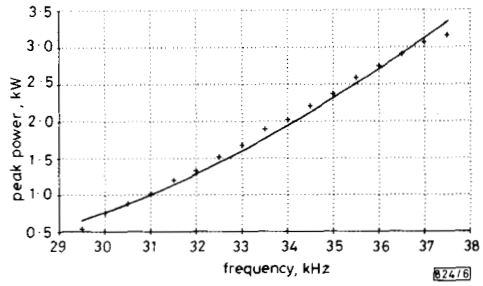

Fig. 6 *Peak power against frequency*
\+ experimental
——— theoretical

Higher frequency and higher power output units are at present under investigation.

J. M. LEISTEN
A. K. LEFEDJIEV*
L. HOBSON

Electrical and Electronic Engineering Department
Brighton Polytechnic
Moulsecoomb, Brighton BN2 4GJ, United Kingdom

21st February 1990

* British Council Sponsored Researcher from Higher Institute of Electrical and Mechanical Engineering, Gabrovo, Bulgaria

References

1 OMORI, H., NAKAOKA, M., YAMASHITA, H., and MARUHASHI, T.: 'A novel type induction heating single-ended resonant inverter using new bipolar Darlington transistor'. Proc. 16th IEEE Power Electronics Specialists Conf., 1985, pp. 590–599
2 LEISTEN, J. M., and HOBSON, L.: 'An assessment of a class E induction cooking unit using a GTO'. Proc. 18th Power Conversion and Intelligent Motion Conference, 1989, pp. 329–353

AUTOREGRESSIVE MODELLING OF AN INDOOR RADIO CHANNEL

Indexing terms: Radiowave propagation, Modelling

An autoregressive model for the frequency domain characteristics of indoor radio channels is introduced. It is shown that a second order process is sufficient to represent the important statistical characteristics of the channel both in the frequency and the time domains. A comparison is made between the statistical characteristics of the empirical data and of the channel responses regenerated from the model.

Introduction: Wideband characterisation of the indoor radio channels has attracted tremendous attention in the recent years. Numerous time-domain measurements for various buildings[1,2,4] and limited frequency domain measurements[3] have been reported. The RMS delay spread of the time domain data and the 3 dB width of the frequency correlation function have been examined in these measurements. These parameters are inversely proportional,[3] and are necessary for the calculation of the data rate limitation of the channel. The cumulative distribution function (CDF) of these parameters for various buildings are available in the literature.[1–4]

The next challenge in this area was to develop a statistical model for computer simulation of the channel to evaluate the different communication techniques. The first model in the time-domain was introduced in Reference 2 and later on improved in Reference 4. The model in Reference 2 is shown to approximately reproduce the CDF of the RMS delay spread of the channel.

We show that the frequency domain measurements of the channel can be represented with an autoregressive model. Additionally, we show that such a model can reproduce close results for the CDFs of the 3 dB width of the frequency correlation function and the RMS delay spread of the channel. The advantage of this model over the time domain models is that it uses fewer parameters. It can therefore be simulated on the computer with considerable ease.

Autoregressive modelling: Fig. 1 shows a sample frequency response of the indoor radio channel measured with a network analyser.[3] The measurement has been made at a set of evenly spaced frequencies

$$f_n = f_0 + nf_s \tag{1}$$

where $f_0 = 900$ MHz is the lowest frequency in the band of study and $f_s = 0{\cdot}25$ MHz is the frequency sample spacing. Assuming an autoregression model for the measured frequencies we have

$$H(f_n, x) = \sum_{i=1}^{p} a_i H(f_{n-i}, x) + V(f_n) \tag{2}$$

where $H(f_n, x)$ is the nth sample of the complex frequency domain measurement at location x, p is the order of the model, and $V(f_n)$ is a complex white noise sequence. The

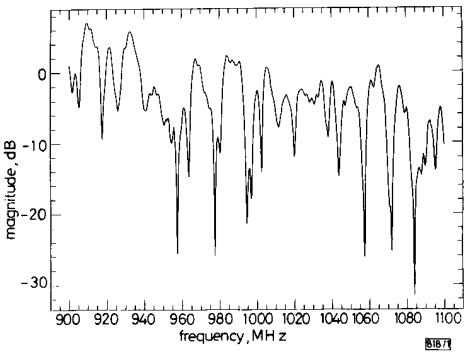

Fig. 1 *Frequency response measurement*

parameters of the model are the coefficients of the linear filter, a_i, that predicts the value of $H(f_n, x)$ based on previous values. Autoregressive modelling of the time domain data used for spectral estimation and the techniques for determination of the coefficients of the AR process are well known.[5]

In the AR modelling of the channel it is assumed that the observed samples of the process are the outputs of a linear filter with transfer function

$$G(z) = \frac{1}{1 - \sum_{i=1}^{p} a_i z^{-p}}$$

driven by a white noise signal $V(f_n)$. This filter is also represented by the p poles in the complex z-plane. Having solved for a_i, one sample of the random process $H(f, x)$ can be generated from eqn. 2 using a random sequence $V(f_n)$.

To determine the validity and the order of the model more than 300 frequency domain measurements were analysed at model orders up to 10. Typically, the magnitude of the largest pole was 0·95 or greater, the second pole was between 0·6 and 0·95, and the magnitude of the remaining $p - 2$ poles were around 0·5 making them insignificant. A scattered plot of the poles that resulted from a 5th order process for the 70 measurements taken in the IBM office at Worcester, MA, USA is shown in Fig. 2.

In the conventional parametric spectral estimation, a pole close to the unit circle represents significant power at the frequency related to the angle of the pole. The frequency is calculated as $f = \arg(z_i)/2\pi T_s$, where T_s is the sampling time.

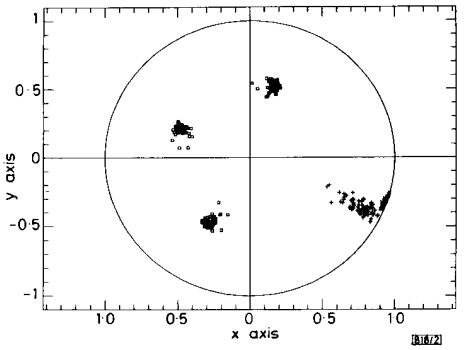

Fig. 2 *Complex z-plane plot of poles for an AR model*